Physicochemical differences after densifying radio frequency plasma sprayed hydroxyapatite powders using spark plasma and conventional sintering techniques

J.L. Xu[†, 1], K.A. Khor [1], R. Kumar[2]

[1] School of Mechanical & Aerospace Engineering, Nanyang Technological University, 50 Nanyang Avenue, Singapore 639798

[2] Department of Environmental Engineering, Montana Tech of the University of Montana, 1300 West Park Street Butte, MT USA 59701

Abstract

The aim of this comparative study was to elucidate the characterization of spherical radio frequency (RF) plasma sprayed hydroxyapatite (HA) powder consolidated by spark plasma sintering (SPS) and conventional sintering methods. SPS processing took place under low vacuum of 4.5 Pa at the temperature of 900-1200 ℃ for 3 min with a heating rate of 100 ℃/min. The conventional processing was conducted at the temperatures of 1000-1400 ℃ in dilatometer furnace in the nitrogen for various periods (2 h and 5 h) with various heating rates (5 ℃/min, 10 ℃/min and 20 ℃/min). The scanning electron microscope (SEM) images of the microstructure revealed a similar morphology obtained in the sample consolidated by conventional processing at 1100 ℃ with a dwell time of 2 h when compared with the sample prepared at 900 ℃ for 3 min using SPS technique. It was found that HA was the dominant phase in the samples densified to above 90% of relative density using SPS technique at the temperatures between 1000 ℃ to 1200 ℃. As a comparison, a maximum density of 2.86 g/cm^3 was achieved using the conventional method at 1200 ℃ with a dwell time of 5 hrs. A large amount of tetra-calcium phosphate (TTCP) and α/β-tricalcium phosphate (α/β-TCP) was detected in the ceramic samples consolidated using the conventional process. This comparison of SPS with conventional sintering showed that the former to be an effective fabrication process for spherical HA powder with optimized microstructure and phase composition.

Keywords: *Radio frequency plasma; Hydroxyapatite; Spark plasma sintering; Conventional sintering*

[†] Corresponding author Tel: 65 6790 4349 fax: 65 6792 4062 E-mail: jlxu@ntu.edu.sg

1. Introduction

Dense and spherical powders are needed for many applications in industry [1-3]. The spheroidisation process might increase the bulk density and improve the “fluidity” of flaky powders. Thus, it facilitates powder handling and allows precise control of powder feed rates in a wide range of applications especially for the thermal spraying. A radio frequency (RF) plasma spheroidisation is the technology of preference for achieving the production of highly spherical and dense powders as it takes full advantage of the inherent features of induction plasma discharge such as providing long plasma residence times [1]. A spherical biomaterial, hydroxyapatite (HA) has been prepared by Bouyer et al. using a RF thermal plasma technology [3].

HA has been a study focus for several decades due to its excellent biocompatitbility and bioactivity for bone substitution and augmentation [3,4]. Its *in vitro* bioactivity (formation of apatite layer) stemmed from the chemical similarity with the apatitic component of natural bone [5]. However, the application of synthetic HA based material in solid form has been limited due to its insufficient mechanical properties. Dense HA capable of withstanding mechanical load depends on the size, morphology and porosity of the staring powders. It has shown that a spark plasma sintering (SPS) technology can consolidate spherical HA to 98-100% relative density in several minutes [6]. During the SPS process, a powder compact can be sintered at a lower temperature than that for conventional sintering. This should be attributed to *in situ* particle surface activation and purification by the spark plasma generated during the process. Therefore, a heat-transfer and mass-transfer between the particles can be completely instantaneously. Four factors that contribute to the fast densification process have been identified as: (i) rapid heat transfer, (ii) the application of a mechanical pressure, (iii) the use of fast heating and cooling rates, and (iv) the use of a pulsed direct current, implying that the samples are also exposed to an electric field [7].

However, the comparison of the densification behaviors of HA based ceramic using various sintering technology is lacking at present. The present study aims to elucidate the sintering differences of RF plasma spheroidized HA powders using SPS and conventional sintering techniques. It attempts to do so considering the microstructure and phase

compositon of the starting powders and final sintered compacts. To achieve this, the RF plasma processed calcium phosphate powders were sintered via spark plasma sintering and in a dilatometer with careful sample control and continuous monitoring. The microstructure, phases present and density in the sintered samples were characterized to compare the results from the SPS process with those from the latter.

2. Materials and sample preparation

The spray formed HA powders were spheroidized in an inductively coupled RF plasma at a plate power level of 21 kW. The starting powder feed rate was set as 5.4 g/min. The other parameters have been stated in previous work [6].

To prepare the conventional sintered HA sample, the starting spherical HA powder was uniaxially pressed into 10 mm diameter pellets utilizing a hydraulic press. The green compacts were prepared under moderate pressures of 200 MPa for 1 min at room temperature to avoid high residual in the powders. In order to eliminate the effects of additives, compaction was performed without binder or other sintering aids. The green compacts (~2.19 g/cm^3) were sintered using a push rod type dilatometer (Netzsch DIL 402C, Germany) at various parameters that were tabulated in Table 1. Nitrogen was used as a protective gas with a flow rate of 50 ml/min. The shrinkage was also measured in the axial direction and the sample support, Netzsch measuring unit, and the displaceable furnace of the dilatometer was mounted horizontally. Length changes were measured with a transducer, which was maintained at a constant temperature by means of water circulation from a constant temperature bath. A calibrated thermocouple placed directly above the sample was used to measure the temperature. To minimize the effect of pressure, only a small force of 0.2 N was applied to the sample through the push rod to maintain contact with the sample. The temperature profile program was controlled by a computer with a data acquisition system. Expansion corrections of the system were taken into account by an identical run using a standard sample (Al_2O_3).

A spark plasma sintering system (Sumitomo Coal Mining SPS system, Dr. Sinter Modal 1050, Japan) was used to prepare SPS consolidated HA compacts. The as-sprayed powders

were loaded in a graphite die (13 mm in diameter) and punch unit. A low pressure was initially applied. The vacuum level of the chamber was 4.5 Pa for powder densification, and the applied compression was 25 MPa. The powder was first heated to 600 ℃ (the lowest controllable temperature of SPS) at the heating rate of 200 ℃/min and then heat up to the set temperatures at various heating rate as listed in Table 1. After holding the powders at a desired temperature and pressure, the applied electric current was stopped, pressure was released, and the sample was cooled to 600 ℃ at a cooling rate of 100 ℃/min and subsequently furnace cooled to room temperature.

3. Characterization

Microstructural analysis was examined using a scanning electron microscope (SEM, JEOL JSM-5600 LV, Japan). The phases present were analyzed by X-ray diffraction (XRD) that was carried out utilizing CuK_{α} Ni filtered radiation at 30 kV and 20 mA on a Philips MPD 1880 diffractometer (the Netherlands). The scanning range (2θ) range was 20 °-60 ° and the scan rate 0.02° s^{-1}. Raman spectra were measured with a Renishaw Raman Imaging Microscope (UK) to examine the bond energies of functional groups in the calcium phosphate present. Data in the range of 800-4000 cm^{-1} was recorded at room temperature and atmospheric pressure. The excitation source was formed by a 632 nm line of a HeNe laser that was attached to the microscope to provide a confocal illumination of the sample via a holographic beam splitter. The densities of the compacts were obtained by Archimedes' principle using de-ionized water as the immersion medium. An ADA 210/L balance (Adam Co. Ltd., UK) equipped with density kit and analysis software was used for the calculations.

4. Results

4.1. Characteristics of feedstock powders

The morphology of the starting RF plasma spheroidized HA powder was shown in Fig. 1 (a). The powders consisted of two particle size distributions: (1) micron-sized and (2)

nanometer sized particles. The average particle size of the powder was found to be ~12 μm. The micron-sized particles were composed of hard agglomerates of fine crystallites that were typically spherical after RF plasma spraying. Due to the size effect and van der Waal's forces, the nanometer-sized particles were attracted to the surface of the larger ones. The soft agglomerates in the nanoparticles might break up easily during compaction.

XRD analysis showed that the starting spherical powder contained not only HA phase but other calcium phosphate phases including α-TCP, TTCP and CaO, as presented in Fig. 1(b). The observed peak broadening could be attributed to the presence of ultrafine particles in the powder. The Raman spectrometry analysis [6] indicated that these RF plasma spheroidized powder was actually in dehydrated state. HA has been partially transformed into oxyhydroxyapatite ($Ca_{10}(PO_4)_6(OH)_{2-2x}O_x$) and possibly, oxyapatite ($Ca_{10}(PO_4)_6O$). Moreover, large amount of amorphous phase (~70 wt.%) has been detected in the nanometer sized particles [8].

4.2. Densification behavior

The densification behavior of the synthesized powder in the SPS system has been investigated and discussed in our earlier work [6], which indicated that shrinkage occurred at about 900 ℃ and continued high to 1150 ℃. The maximum shrinkage rate was achieved at 1060 ℃. Fig. 2 shows the shrinkage results of the RF plasma spheroidized powders sintered at various conditions. It was found that two steps of shrinkage were observed the densification characteristics through dilatometer during sintering at 1300 ℃. The first slight shrinkage up to around 200 ℃ corresponded to the effect of water elimination resulting in the volume contraction. The second shrinkage, starting at around 500 ℃, represented the sintering period, from which the best densification range could be determined. Above this temperature, significant shrinkage starts to take place. As shownin Fig. 2, the densification in the SPS system starts at around 920–950 ℃ at the various heating rates. The starting sintering temperature increased slightly up to about 940 ℃ as increasing heating rates from 50 ℃/min to 200 ℃/min.

4.3. Effects of sintering temperatures

Fig. 3(a)-(d) showed the SEM images of the various samples surface sintered at various temperatures in the dilatometer. As shown, all these obtained ceramics were quite porous. At the sintering temperature of 1100 ℃ (Fig. 3(a)), a non-uniform sintering profile was observed. It was found that the formation and growth of neck occurred between the ultrafine particles. The larger particles were not densified or undergo limited densification. When the sintering temperature was increased to 1200 ℃, the particles in the micrometer range began to sinter more effectively. To decrease the numbers of boundaries as well as the free surface, the fine grains formed from the nano particle merged into the micron sized ones (shown in Fig. 3(b)). Further increasing the sintering temperature to 1300 ℃ resulted in an apparent rise in densification. Subsequently, the pores gradually diminished due to the driving force from temperature. But they still existed in the form of continuous open porosity. Sintering at 1400 ℃ led to relatively denser microstructure when compared with the samples sintered at low temperatures. The linked pores became relatively smaller and were partially reduced to closed pores.

As a reinforcement of our previous work [6], similar microstructures in the SPS samples were achieved at 900 ℃ with a dwell time of 3 min (Fig. 3(a)) when compared with the samples prepared at 1100 ℃ for 2 h in the dilatometer. Nearly fully densification of the samples has been achieved at the sintering temperature of 1000 ℃ with a density of 3.00 g/cm^3. The densities of the samples after sintering at 1100 ℃ and 1150 ℃ were 3.04 g/cm^3 and 3.05 g/cm^3 , respectively.

Fig. 4 showed the XRD patterns of the ceramics sintered at various temperatures for 2 h at a heating rate of 5 ℃/min in the dilatometer. HA, TTCP and a mixture of both α- and β-TCP were observed in the obtained ceramics that were fired below 1200 ℃. Upon increasing sintering temperatures above 1300 ℃, α-TCP and TTCP were predominant in the consolidated samples. As a comparison, HA was the dominant phase and β-TCP was also observed in the SPS samples. α-TCP was detected in the samples prepared at above 1150 ℃ in the SPS system [6].

The presence of various calcium phosphate phases influenced the dilatometer consolidated sample densities. Table 1 summarized the obtained density of each sample in relation to the sintering temperatures. The sintering density had an initial increase followed by a subsequent decrease with increasing the temperature.

4.4. Effects of heating rate

The comparative XRD results (Fig. 5) obtained from the dilatometer and SPS system revealed an interesting effect of heating rates on the evolution of the various calcium phosphate phases. It was found that HA was a dominant phase in the consolidated samples. However, TTCP was detected in the samples consolidated at the heating rate of 50 ℃/min and below. Compared to the peak of HA, the relative peak intensities of TTCP decreased with an increase in the heating rates. This result indicated that heating rate had an influence on the transformation behaviors of different calcium phosphates in the starting RF plasma sprayed powders. Empirically the TTCP could be minimized at high heating rate of 200 ℃/min. However, too high heating rate is suggested to be avoided during sintering as it may damage the heating elements of the sintering system.

Raman spectra taken from the surface of the pellets (Fig. 6) indicated that the sintering procedure has a minor influence on the chemistry of the samples. The effect exhibited by the different heating rates on the peaks position detected might be attributed to the compositional re-organization of different HA phases in the ceramics. The peak at ~960 cm^{-1} was assigned to P-O stretching mode (ν_1) of the PO_4 group and the peak at ~962 cm^{-1} refers to P-O stretching mode (ν_1) in HA. The shoulder peak at ~950 cm^{-1} corresponded to the presence of TCP [11]. No stretching signal belonging to OH in HA was observed which suggested that the consolidated samples were still in dehydrated state and few hydroxyl was recovered into the apatite structure during sintering.

Fig. 7(a)-(c) showed the surface SEM morphology changes of the samples prepared via dilatometer, whose grain sizes were within several micrometers. Due to the high surface energy associated with the nano particles they were consumed by the larger particles at relatively lower temperature (~500 ℃) during sintering. Though the grain size was not

rigorously determined for the sample sintered at the heating rate of 5 ℃/min, a gradual decrease in grain size was still observed under SEM with an increase in the heating rates. From visual observation the smallest grain size in all samples was rather similar at about 1 μm.

It was also obvious that the compacts processed at the various heating rates in the dilatometer at 1200 ℃ for 5 h were not fully sintered, and the sample prepared at 5 ℃/min contained extensive open porosity. At the heating rate of 10 ℃/min, an average grain size of 3.5 μm and some closed pores were noted. This trend continued for the sample prepared at the heating rate of 20 ℃/min and the average grain size decreased to about 2.5 μm.

The effect of heating rate on the grain sizes was clearly evident for the sample sintered using SPS. After polishing, no obvious pores could be detected in the SPS sintered specimen without etching (Data not shown). However, after etching in 3 vol.% nitric acid for 10 s, not only grains but porosity was also observed. As shown in Fig. 7 (d), a relatively uniform microstructure with the average grain size of 0.5 μm was exhibited by the sample sintered at 1100 ℃ with a dwell time of 3 min using SPS. The particles also had a fully developed neck structure. These well-defined surface facets denoted the final sintering geometry. In this case, the extensive interconnectivity between the particles prevented substantial consolidation. Therefore, the grain size after spark plasma sintering did not grow appreciably as compared to conventional sintering (dilatometry studies). Fig. 7(e) presents that relatively larger grains were achieved at the sintering temperature of 1200 ℃ when compared with the grains of the sample prepared at 1100 ℃ using SPS. This observation is consistent with the previous fracture surface study [6] that showed the grains became coarsening obviously at a higher SPS temperature of 1200 ℃.

Fig. 8 shows the cross-sectional view of the samples densified at 1200 ℃ for 5 h with heating rates of 5 ℃/min, 10 ℃/min and 20 ℃/min by conventional route. All the three samples showed inhomogeneous pore distribution. As observed, there are many large pores are observed inside the sample densified at a heating rate of 5 ℃/min. It is much more porous than the samples sintered at 10 ℃/min and 20 ℃/min. Moreover, it was found that the outmost region (~30μm) of the sample prepared at 20 ℃/min was relatively denser than those of the samples prepared at heating rates of 5 ℃/min and 10 ℃/min.

The differences in the samples prepared by SPS and conventional sintering were also reflected in sintered density of the compacts (Table 1). The sintered density obtained from the conventional sintering was less than 90% of the theoretical density of HA (3.156 g/cm3). The maximum density of 2.86 g/cm3 was obtained at 1200 ℃ for 5 h with a heating rate of 10 ℃/min. In contrast the sample prepared in the SPS system achieved a near-full density (>3.02 g/cm^3) at the temperature of 1100 ℃ for 3 min at various heating rates.

5. Discussion

The main driving force in sintering was the surface free energy of the particles. It followed that, smaller the particle size, higher the surface free energy, easier the surface atom diffusion between neighboring particles which ultimately lowered the sintering temperature. Correspondingly, the sintering temperature of ultrafine particles was lower than that of larger particles. In the present study, both the fracture surface images of the samples consolidated at 1100 ℃ in the dilatometer and that of the sample prepared at 900 ℃ in the SPS system showed that the ultrafine particles in the starting RF plasma spheroidized powder initially started to sinter at lower temperature than those larger particles.

According to the results, it was observed that the densification in the dilatometer was considerably slower than that consolidated using the spark plasma sintering technology. This phenomenon could be attributed to the unique heating feature of the SPS process [9-11]. In the SPS process, the large electrical current and the apparent plasma induced by the discharge at the micro-gap between the powder surfaces produced the electrons, cations and anions to strike the surface of the opposite particles, which enabled a local high temperature to be created in the contacting areas of the particles resulting in the quick formation of the neck.

It was well documented that the densification depended on the heating rates as well as the soak temperatures in the solid state densification region [12]. Several other studies have revealed that sintering proceeded more rapidly at higher heating rates [13,14]. The ability of conventional theories to explain this fact was that high heating rates minimize the effects of surface diffusion processes not contributing to densification, hence the compact body

reached higher temperatures in a highly sinterable state [15]. The major advantages of using rapid sintering rates may be summarized as following: (a) The grain growth at the early stage of sintering was suppressed and (b) the capillary force between particles increased throughout the densification cycle owing to very limited grain growth. Accordingly, the possibility of high densification was optimized for the rapid SPS process with a heating rate up to 200 ℃/min. However, it should be considered that the effect of dwelling or soak time for the densification as a longer sintering duration would also results in relatively denser sample at the same sintering temperature [16].

According to Bomlai et al. [16], a relative high density was expected to achieve at a higher heating rate using conventional sintering route. It is clearly seen that density increased as heating rate increased from 5 ℃/min to 10 ℃/min reaching of a value of 2.86 g/cm^3 at 10 ℃/min. However, the sample prepared at 20 ℃/min gave a relatively small density of 2.77 g/cm^3 as compared with that of the sample prepared at 10 ℃/min. It was reported that the higher sintering rate accompanied higher thermal gradients between the surface and the center of a sample [17]. The temperature gradients held over a period of time could provide a new driving force of sintering. In other words, the outer most region of the sample might be densified much faster than the core due to the thermal gradients if the densification rate exceeds the rate of heat transfer [17]. Fig. 8 shows that the outmost region of the sample prepared at 20 ℃/min is relatively denser than the core part. For the samples densified at 10 ℃/min and below, relatively homogeneously distributed pores were detected. When the densification rate of the exterior of the sample was much greater, the inside of the sample might not be able to densify as well because the outer skeleton exerted geometrical constrains on densification. As a result the possibility of larger pores left inside the densified ring increased. Alternatively, as proposed by Ryu et al. [18], the densification at a high heating rate in the solid phase was by rearrangement of the primary particles instead of the surface area changes. This would then result in insufficient shrinkage of the sintered sample thus decreasing overall density. As such when compared with the heating rate at 10 ℃/min, the drop in density at the heating rate of 20 ℃/min could be attributed to the presence of larger pores inside the sample. While at heating rate of 10 ℃/min, the heating up period became relatively longer as compared with that heated at heating rate of 20 ℃/min.

In addition, the role of heating rate on phase formation especially the non-stoichiometric apatite in the starting powder should be taken into account in the present study. The reactions below 1200 ℃ at low partial pressure of water vapor were generally controlled in calcium phosphates by the following equations [19]:

$$2Ca3(PO4)2 + Ca_4P_2O_9 \rightarrow Ca_{10}(PO_4)_6O \quad (1)$$

$$Ca_3(PO_4)_2 + CaO \rightarrow Ca_4P_2O_9 \quad (2)$$

When the temperature reached 1200 ℃, however, the non stoichiometric apatite in the starting powder was reactive and might decompose into other compounds given as:

$$Ca_{10}(PO_4)_6O \rightarrow 2Ca_3(PO_4)_2 + Ca_4P_2O_9 \quad (3)$$

Therefore, various levels of calcium phosphates were observed in the final samples due to the combined physico-chemical reactions (1)-(3). Since a low heating rate increased the sintering stage, the longer duration could enhance decomposition of non-stoichiometric apatite into TTCP and TCP which also had lower densities than stoichiometric HA. Therefore, a longer heating period at 5 ℃/min resulted in the more decomposition from oxyapatite into TTCP and TCP. That is, due to the combined effect of heating rate on densification and phase composition, the higher densitywas achieved from the sample prepared at 1200 ℃ for 5 h at a heating rate of 10 ℃/min, not from the samples sintered at heating rates of 5 ℃/min and 20 ℃/min, as shown in Table 1.

As for the spark plasma sintered sample, it showed a relatively higher sintered density and relatively fine grain sizes compared with samples prepared by the conventional route. Not only should the above mentioned effects of heating rates on densification behavior be considered, but also the mechanism of spark plasma sintering addressed. As discussed previously, the most important characteristic of SPS was that it was controlled by the current and pulse cycling rate. Also, there were no insulators and heating elements of large heat capacity. The discharges were generated by an instantaneous pulsed direct current that was applied through electrodes at the top and bottom punches of the graphite die. Therefore, the powder was heated by spark discharges in voids between the particles. As a result, the sample can be sintered uniformly and rapidly to its full density from both inside and outside with few pores in contrast with samples prepared by conventional sintering method. Furthermore when the consolidation was completed in a few minutes (including

heating/cooling and holding stages), the grain growth was efficiently minimized [20]. In addition, by using SPS technique, deleterious decomposition reactions (for example, Eq. (3)) could be suppressed and even avoided. Furthermore, TTCP was not detected within the detectable extent of XRD (0.5 wt.%), in the spark plasma sintered samples. This was probably due to two factors: (a) the crystal structure of TTCP was similar to that of HA [20] and (b) TTCP was less stable than both HA and TCP [19]. As such the TTCP present in the RF plasma sprayed powders could have combined with surrounding TCP and given rise to oxyapatite by faster activation of the spark plasma. At the same time it was highly probable that the high temperature polymorph α-TCP from the starting powders transformed into the more stable β-TCP [21] aided by the activation energy available at the higher local temperatures.

6. Conclusion

In this study, we have investigated the effects of temperatures and heating rate on the densification of RF plasma spheroidized hydroxyapatite powders using spark plasma sintering and conventional sintering techniques. The results reaffirmed that grain growth during densification was inescapable using conventional pressureless sintering routes even at relatively higher heating rates. A consolidated HA with a maximum density of 2.86 g/cm^3 was obtained by the conventional process at 1200 ℃ for 5 h with a heating rate of 10 ℃/min. It was also shown that the use of spark plasma sintering effectively densified hard to sinter calcium phosphate powders to a nearly full density of 3.04 g/cm^3 of hydroxyapatite within 3 minutes at the lower sintering temperature of 1100 ℃ with a heating rate of 100 ℃/min. Compared with those samples prepared by conventional route, the spark plasma consolidated samples were substantially denser concomitantly exhibiting finer grain sizes. These results were mainly attributed to the rapid sintering capability of SPS method.

Acknowledgements

This work has been supported by Nanoscience Innovation and Nanyang Technological University (NSI-NTU) joint project.

References

[1] M. Boulos, Metal Powder Rep. 59 (2004) 16–21.

[2] M.I. Bolus, IEEE Trans. Plasma Sci. 19 (1991) 1078–1089.

[3] E. Bouyer, F. Gitzhofer, Boulos MI, IEEE Trans. Plasma Sci. 25 (1997) 1066–1072.

[4] R. Kumar, P. Cheang, K.A. Khor, J. Mater. Process. Technol. 113 (2001) 456–462.

[5] Z. Zyman, I.G. Ivanov, V.I. Glushko, J. Biomed. Mater. Res. 46 (1999) 73–79.

[6] J.L. Xu, K.A. Khor, Y.W. Gu, R. Kumar, P. Cheang, Biomaterials 26 (2005) 2197–2207.

[7] Y. Wang, Z. Fu, Mater. Sci. Eng. A 90 (2002) 34–37.

[8] J.L. Xu, K.A. Khor, Z.L. Dong, Y.W. Gu, R. Kumar, P. Cheang, Mater. Sci. Eng. A 374 (2004) 101–108.

[9] C.H. Shan, S.H. Risbud, Mater. Sci. Eng. B 26 (1994) 55–60.

[10] X. Yao, Z. Huang, L. Chen, D. Jiang, S. Tan, D. Michel, G. Wang, L. Mazerolles, J. Pastol, Mater. Lett. 59 (2005) 2314–2318.

[11] J. Hong, L. Gao, S.D.D.L. Torre, H. Miyamoto, K. Miyamoto, Mater. Lett. 43 (2000) 27–31.

[12] M.B. Holmes, V.A. McCrohan, W.Y. Howng, in: M.F. Yan, A.H. Heuer (Eds.), Additives and Interfaces in Electronic Ceramics, American Ceramic Society, Columbus, 1984, p. 149.

[13] P. Roura, J. Costa, J. Farjas, Mater. Sci. Eng. A 337 (2002) 248–253.

[14] Y. Zhou, K. Hirao, Y. Yamau

[15] D.L. Johnson, in: C.C. Kuczynski, A.E. Miller, G.A. Sargent (Eds.), Mater. Sci. Res., vol. 16, Plenum Press, New York, 1983, pp. 243–252.

[16] P. Bomlai, N. Sirikulrat, T. Tunkasiri, Mater. Lett. 59 (2005) 118–122.

[17] B.C. Kim, J.H. Lee, J.J. Kim, T. Ikegami, Mater. Lett. 52 (2002) 114–119.

[18] S.S. Ryu, Y.D. Kim, I.H. Moon, J. Alloys Compd. 335 (2002) 233–240.

[19] Y. Sargin, M. Kixiyalli, C. Telli, H. Guler, J. Eur. Ceram. Soc. 17 (1997) 963–970.

[20] M. Omori, Mater. Sci. Eng. A 287 (2000) 183–188.

[21] F.H. Lin, C.J. Liao, K.S. Chen, J.S. Sun, Mater. Sci. Eng. C 13 (2000) 97–104.

List of table

List of Figures

Figure 7 SEM micrographs of the RF plasma sprayed powders using different sintering routes: (a–c) show the ceramic surface microstructure of the samples sintered by conventional sintering route at 1200 ℃ for 5 h at a heating rate of 5 C/min, 10 ℃/min, and 20 ℃/min, respectively; (d) shows the etched surface morphology of the sample prepared using SPS at 1100 ℃ for 3 min at a heating rate of 100 ℃/min; (e) presents the etched surface morphology of the sample prepared using SPS at 1200 ℃ for 3 min at a heating rate of 100 ℃/min

Figure 8 SEM micrographs of the cross-sectional view of the RF plasma sprayed powders sintered by conventional sintering route at 1200 ℃ for 5 h at a heating rate of 5 ℃/min (a), 10 ℃/min (b), and 20 ℃/min (c). The scale bar is 50μm

Table 1
Sintering parameters and the sintered densities of the obtained ceramic samples

Sintering temperature and sintering system	Dwell time	Heating rate (°C/min)	Density (g/cm^3)
1100 °C, dilatometer	2 h	5	2.48
1200 °C, dilatometer	2 h	5	2.62
1300 °C, dilatometer	2 h	5	2.53
1400 °C, dilatometer	2 h	5	2.31
1200 °C, dilatometer	5 h	5	2.73
1200 °C, dilatometer	5 h	10	2.86
1200 °C, dilatometer	5 h	20	2.77
1100 °C, SPS	3 min	50	3.02
1100 °C, SPS	3 min	100	3.04
1100 °C, SPS	3 min	200	3.03
1200 °C, SPS	3 min	100	3.04

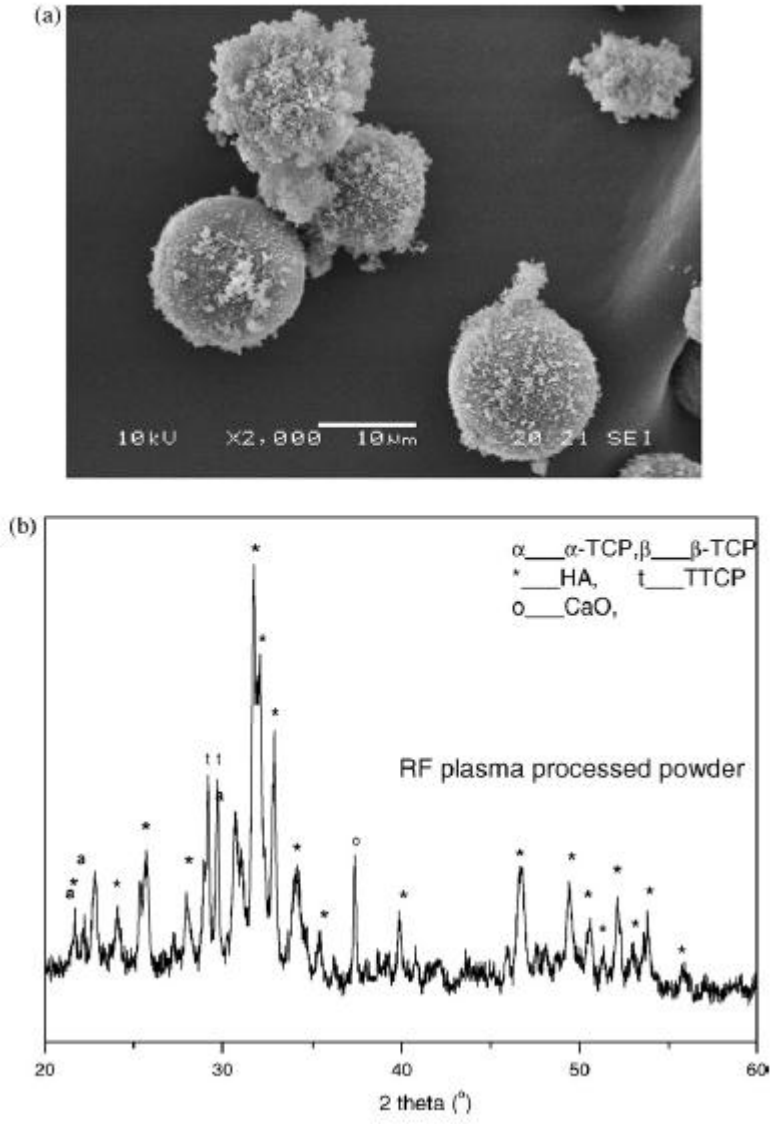
(a)
10kV X2,000 10μm 20 21 SEI
(b)
α___α-TCP,β___β-TCP
*___HA, t___TTCP
o___CaO,
RF plasma processed powder
20
30
40
50
60
2 theta (°)

Fig. 1

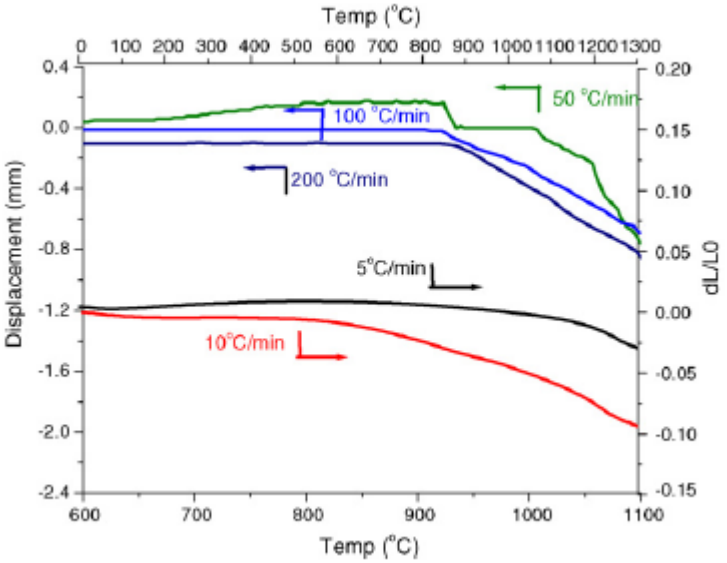
Temp (°C)
0 100 200 300 400 500 600 700 800 900 1000 1100 1200 1300
0.4
0.0
-0.4
-0.8
-1.2
-1.6
-2.0
-2.4
Displacement (mm)
0.20
0.15
0.10
0.05
0.00
-0.05
-0.10
-0.15
dL/L0
50 °C/min
100 °C/min
200 °C/min
5°C/min
10°C/min
600 700 800 900 1000 1100
Temp (°C)

Fig. 2

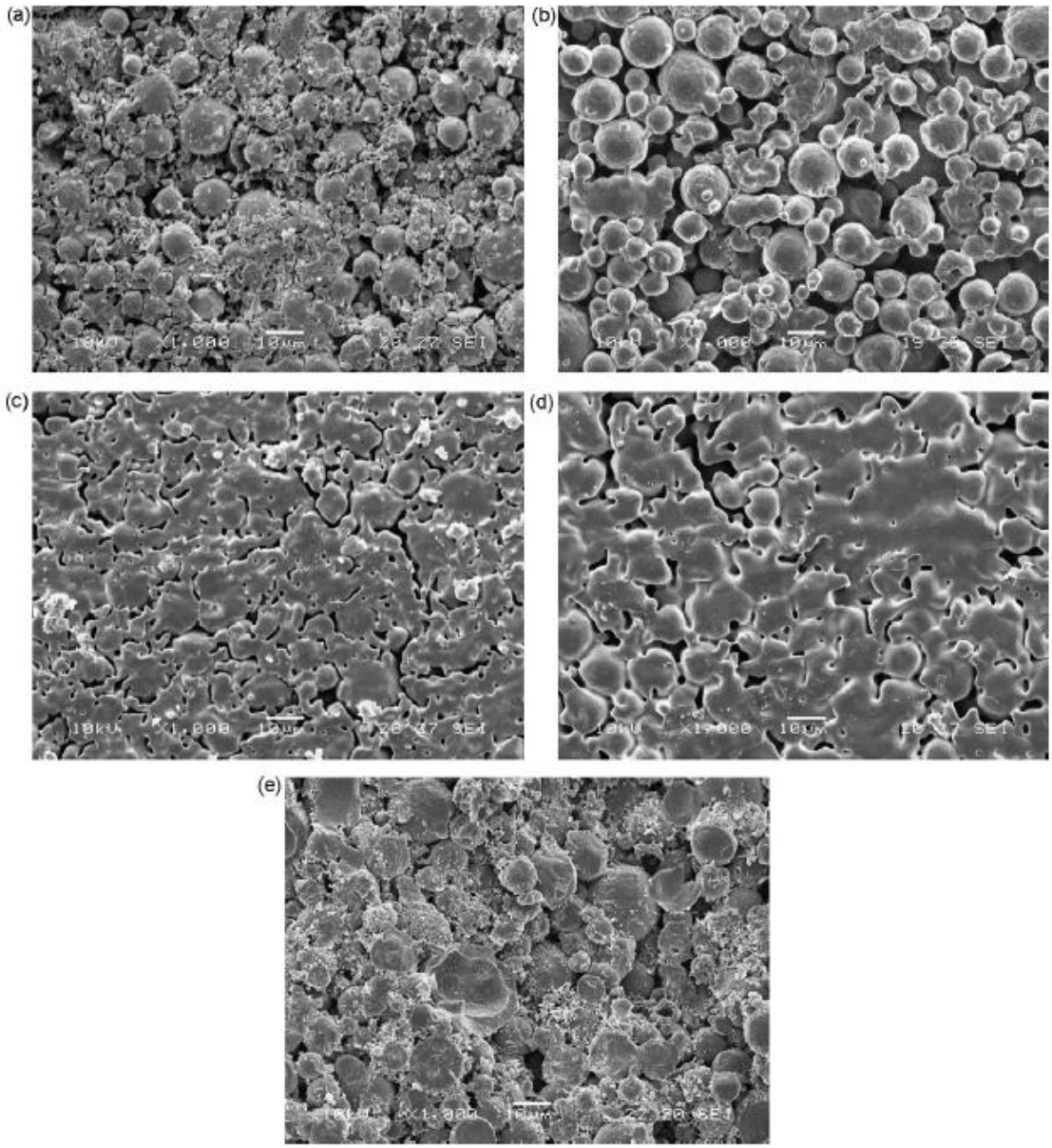

Fig. 3

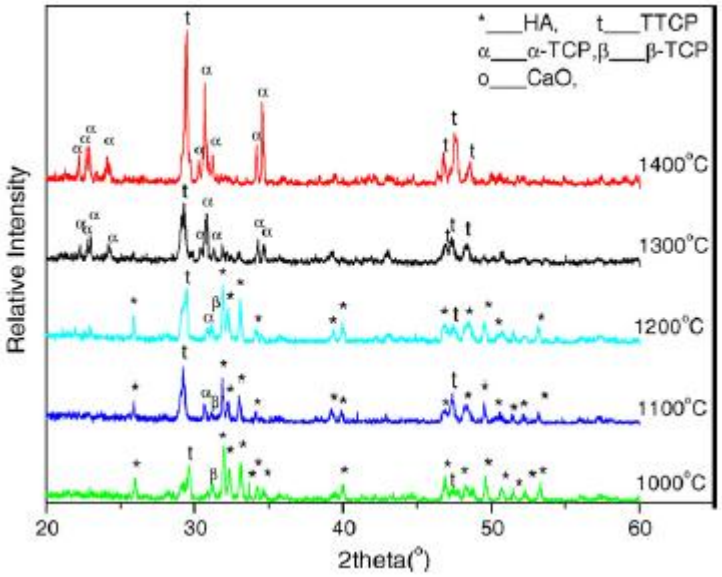
*___HA, t___TTCP
α___α-TCP,β___β-TCP
o___CaO,
1400°C
1300°C
1200°C
1100°C
1000°C
Relative Intensity
2theta(°)
20
30
40
50
60

Fig. 4

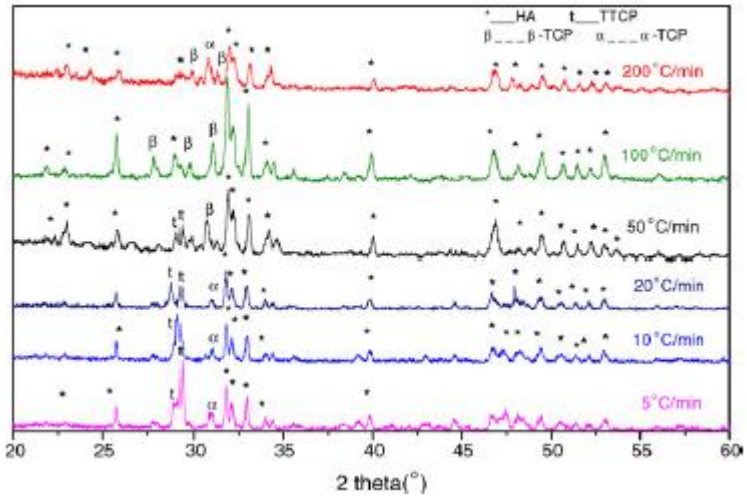
*___HA t___TTCP
β___β-TCP α___α-TCP
200°C/min
100°C/min
50°C/min
20°C/min
10°C/min
5°C/min
20
25
30
35
40
45
50
55
60
2 theta(°)

Fig. 5

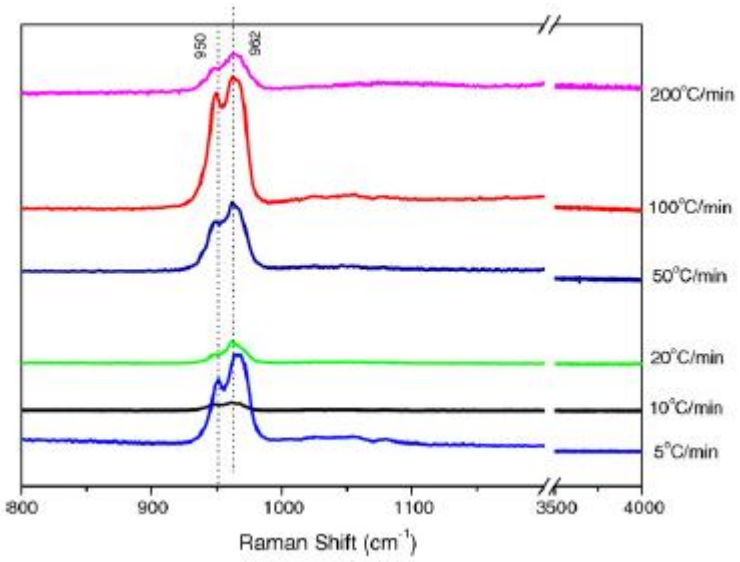
950
962
200°C/min
100°C/min
50°C/min
20°C/min
10°C/min
5°C/min
800
900
1000
1100
3500
4000
Raman Shift (cm-1)

Fig. 6

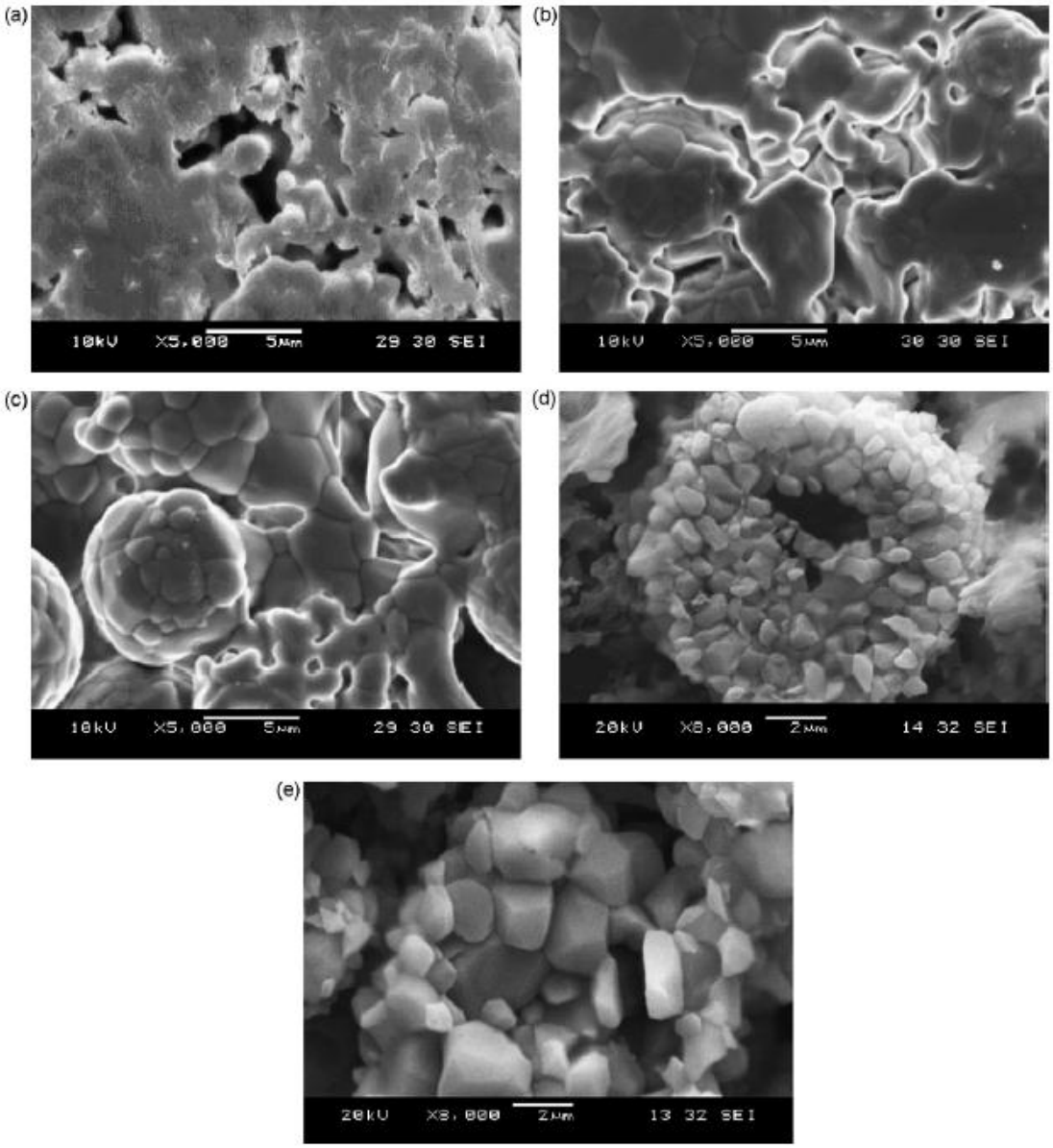
(a)
10kV X5,000 5μm 29 30 SEI
(b)
10kV X5,000 5μm 30 30 SEI
(c)
10kV X5,000 5μm 29 30 SEI
(d)
20kV X8,000 2μm 14 32 SEI
(e)
20kV X8,000 2μm 13 32 SEI

Fig. 7

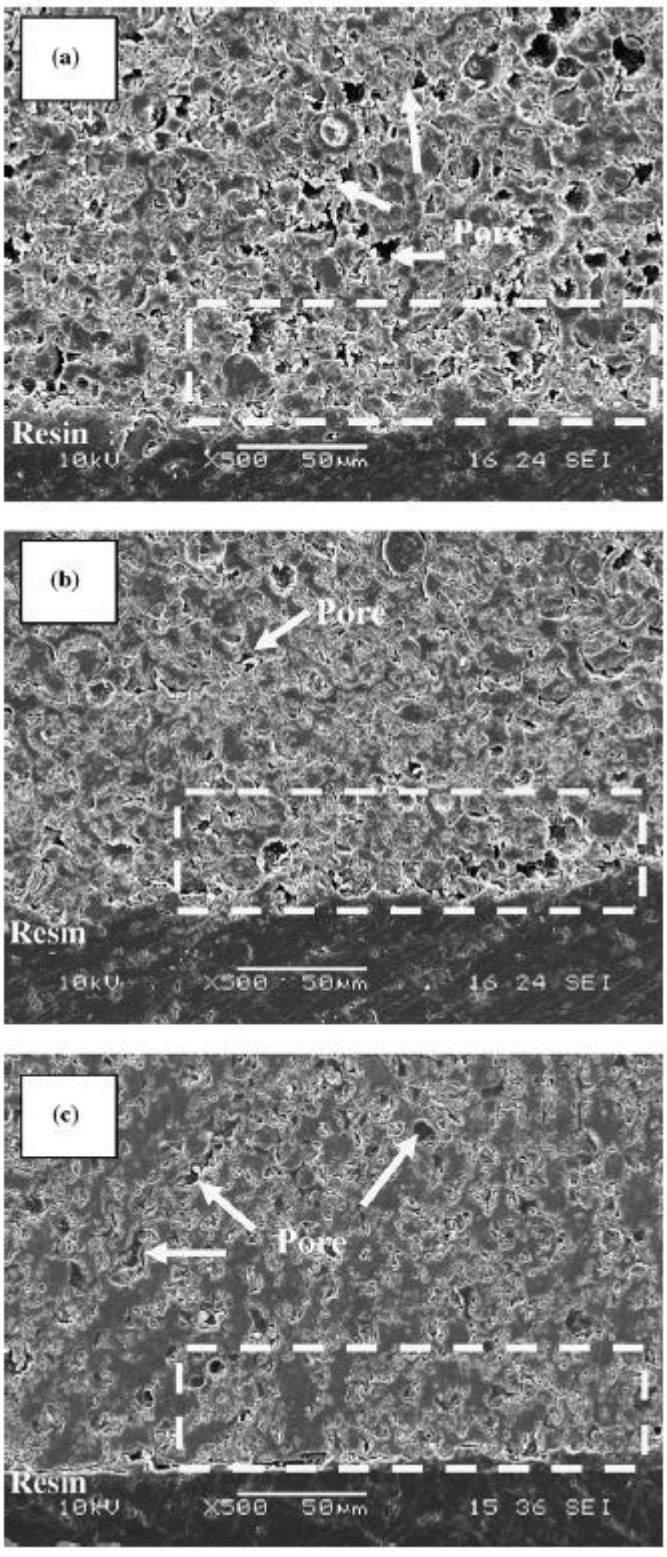
(a)
Pore
Resin
10kU X500 50µm 16 24 SEI
(b)
Pore
Resin
10kU X500 50µm 16 24 SEI
(c)
Pore
Resin
10kU X500 50µm 15 36 SEI

Fig. 8